Nechaev, Anton A.; Gonzalez, Gabriel; Verma, Prachi; Peshkov, Vsevolod A.; Bannykh, Anton; Hashemi, Arsalan; Hannonen, Jenna; Hamza, Andrea; Pápai, Imre; Laasonen, Kari; Peljo, Pekka; Pihko, Petri M.

Exploration of Vitamin B_6-Based Redox-Active Pyridinium Salts Towards the Application in Aqueous Organic Flow Batteries

Published in:
Chemistry - A European Journal

DOI:
10.1002/chem.202400828

Published: 25/06/2024

Document Version
Publisher's PDF, also known as Version of record

Chemistry–A European Journal
Research Article
doi.org/10.1002/chem.202400828
Chemistry Europe
European Chemical Societies Publishing
www.chemeurj.org

Exploration of Vitamin B_6-Based Redox-Active Pyridinium Salts Towards the Application in Aqueous Organic Flow Batteries

Anton A. Nechaev[+],[a] Gabriel Gonzalez[+],[b] Prachi Verma,[a] Vsevolod A. Peshkov,[a] Anton Bannykh,[a] Arsalan Hashemi,[c] Jenna Hannonen,[b] Andrea Hamza,[d] Imre Pápai,[d] Kari Laasonen,[c] Pekka Peljo,*[b] and Petri M. Pihko*[a]

Pyridoxal hydrochloride, a vitamin B_6 vitamer, was synthetically converted to a series of diverse redox-active benzoyl pyridinium salts. Cyclic voltammetry studies demonstrated redox reversibility under basic conditions, and two of the most promising salts were subjected to laboratory-scale flow battery tests involving galvanostatic cycling at 10 mM in 0.1 M NaOH. In these tests, the battery was charged completely, corresponding to the transfer of two electrons to the electrolyte, but no discharge was observed. Both CV analysis and electrochemical simulations confirmed that the redox wave observed in the experimental voltammograms corresponds to a two-electron process. To explain the irreversibility in the battery tests, we conducted bulk electrolysis with the benzoyl pyridinium salts, affording the corresponding benzylic secondary alcohols. Computational studies suggest that the reduction proceeds in three consecutive steps: first electron transfer (ET), then proton-coupled electron transfer (PCET) and finally proton transfer (PT) to give the secondary alcohol. ^{1}H NMR deuterium exchange studies indicated that the last PT step is not reversible in 0.1 M NaOH, rendering the entire redox process irreversible. The apparent reversibility observed in CV at the basic media likely arises from the slow rate of the PT step at the timescale of the measurement.

Introduction

In recent years, the amount of electrical energy generated from intermittent renewable sources has been continuously increasing.[1] This boosts the demand for the production of energy storage facilities of medium and large scales. Flow Batteries (FBs) are viewed as one of the most promising technologies for solving this issue.[2] A unique opportunity to tailor the electrode surface area as well as the volume and concentration of a working electrolyte is deemed to be the key for incorporating such batteries to variously sized electrical grids.

Classical and well-developed Vanadium Flow Batteries (VFB) represent a significant part of a commercially implemented batteries of this type.[3] Despite their great stability, the price of raw materials and the toxicity of electrolytes prompt researchers to search for alternative solutions.[4] Accordingly, Organic Flow Batteries (OFB) have been introduced as the next-stage opportunity for large-scale electrical energy storage. Low prices, accessibility, and abundance of organic electroactive materials could make OFB financially more attractive in a long-term perspective. Recently, special attention has been paid to Aqueous Organic Flow Batteries (AOFBs) – water-based, non-flammable, and easily maintained OFBs sub-division.[5] Utilization of aqueous electrolytes offers the safest and cheapest settings for FBs implementation on industrial scale. Anthraquinones,[6] TEMPO-derivatives,[7] fluorenones,[8] flavins[9] are among the most prominent molecules used in aqueous electrolytes that have been developed to date. Despite substantial progress in this area, the search for new cost-effective, safe, and scalable water-soluble redox-active organic molecules for AOFBs continues.[10]

Pyridinium salts occupy a significant niche in organic chemistry.[11] Known as redox-active functional group transfer

[a] Dr. A. A. Nechaev,[+] Dr. P. Verma, Dr. V. A. Peshkov, A. Bannykh, Prof. Dr. P. M. Pihko
Department of Chemistry, University of Jyväskylä, P.O. Box 35, Jyväskylä, 40014, Finland
E-mail: petri.pihko@jyu.fi

[b] G. Gonzalez,[+] J. Hannonen, Prof. Dr. P. Peljo
Research Group of Battery Materials and Technologies, Department of Mechanical and Materials Engineering, Faculty of Technology, University of Turku, Turku, 20014, Finland
E-mail: ekka.peljo@utu.fi

[c] Dr. A. Hashemi, Prof. Dr. K. Laasonen
Department of Chemistry and Material Science, School of Chemical Engineering, Aalto University, Espoo, 02150, Finland

[d] Dr. A. Hamza, Prof. Dr. I. Pápai
Institute of Organic Chemistry, HUN-REN Research Centre for Natural Sciences, Magyar tudósok körutja 2, Budapest, 1117, Hungary

[+] Denotes equal contribution.

Supporting information for this article is available on the WWW under https://doi.org/10.1002/chem.202400828

reagents for a variety of chemical transformations,[12] it is not surprising that *N*-functionalized pyridinium scaffolds were identified as promising candidates for redox-active materials in FBs. In particular, promising results have been achieved with bipyridinium-based viologens[13] and diquats,[14] benzoyl-substituted pyridinium ions (in both non-aqueous[15] and aqueous[16] media) and pyridinium-carbene hybrids.[17]

A realistic flow battery material should also be available in sufficient quantities, ideally from natural sources. Among the pyridine-based biobased molecules, vitamin B_6 was viewed as a highly promising candidate. Vitamin B_6 comprises a series of six pyridine-based chemically related derivatives, so-called "vitamers" that are interconvertible in living systems, with the pyridoxal 5′-phosphate being an active form (Figure 1).[18] All B_6 vitamers are water soluble, available via fermentation,[19] and likely to possess high biodegradability. All these properties are highly advantageous for prospective AOFB molecules. Furthermore, the presence of pre-installed functional groups renders B_6 vitamers excellent candidates for a broad synthetic exploration.[20,21,22,23]

In our previous study, we described the development of a computational protocol that combines semiempirical and DFT quantum chemical methods to predict the redox potentials as well as the stability of reduced species of perspective vitamin B_6-based aqueous electrolytes.[24] The outlined framework revealed the set of vitamin B_6 derivatives with the predicted redox potentials falling within the electrochemical stability window of water.[25] Herein we report a general synthetic platform to access a wide range of water-soluble *N*-alkylated benzoyl pyridinium salts based on vitamin B_6 as well as the experimental assessment of their electrochemical behaviour and performance in flow batteries.

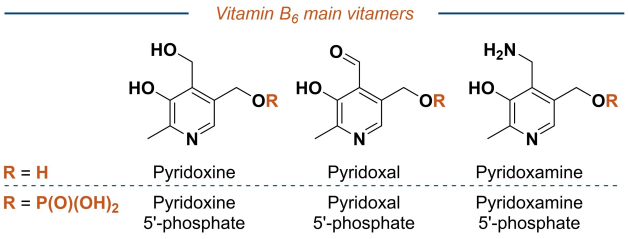

Figure 1. Vitamin B_6 vitamers.

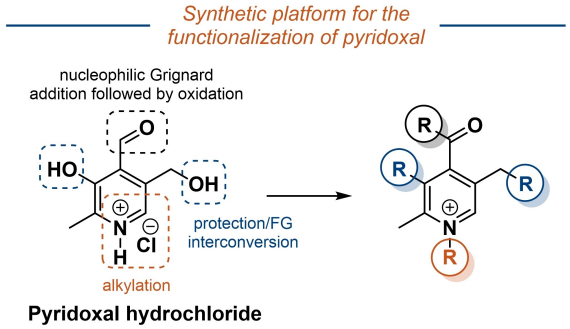

Scheme 1. Outline for the synthetic elaboration of pyridoxal hydrochloride.

Synthetic Modification of the Vitamin B_6 Core

We have chosen commercially available pyridoxal hydrochloride, the oxidized form of vitamin B_6 as a starting point for synthetic exploration. The proposed outline is shown in Scheme 1 and involves the nucleophilic Grignard addition to the aldehyde group followed by the oxidation to introduce a benzoyl pyridine motif. Phenolic and benzylic hydroxy groups that would likely require protection during the implementation of the above sequence can later be used for generating more derivatives via functional group interconversion. In the final stage, the alkylation of pyridine nitrogen enables formation of pyridinium salts.

The initial attempts to functionalize carbonyl group with phenyl magnesium chloride failed likely due to the insolubility of pyridoxal in organic solvents. Accordingly, installing lipophilic silyl groups has been proposed as a convenient solution to increase the solubility of pyridoxal and to avoid an interference of unprotected OH groups with the Grignard reagent. Treating pyridoxal hydrochloride with *tert*-butyldimethylsilyl chloride in the presence of DABCO in acetonitrile led to the formation of bis-silylalted pyridoxal ether **1** in 97% of yield (Scheme 2). Subsequent functionalization of **1** with phenyl magnesium chloride gave a rise to secondary alcohol **2** in 78% of yield. Oxidation of **2** with Dess–Martin periodinane in dichloromethane led to the formation of benzoyl pyridine **3** in 55% of yield. *N*-alkylation of pyridoxoketone **3** was performed using appropriate iodoalkanes in DCM at 50 °C and was accompanied by a partial desilylation at the phenolic OH group yielding monosilylated benzoyl pyridinium salts **4a** and **4b** with the latter being obtained in a mixture with bis-silylated pyridinium salt **4′**. Treating compounds **4** with ammonium fluoride in methanol at rt provided zwitter-ionic pyridinium derivatives **5a** and **5b** in good yields with the structure of **5b** being confirmed by a single crystal X-Ray diffraction (XRD) analysis (CCDC 2325623).

Subsequently, compounds **5a–b** were subjected to electrochemical studies, but voltammetry tests showed a non-reversible reduction process at a very negative potential close to water reduction (see electrochemical exploration for details).

Therefore, we devised a new synthetic route that rules out the formation of zwitterionic compounds (Scheme 3). The key idea was to expose the phenolic OH group via partial deprotection of bis-silylated pyridoxal **1** and then block it via *O*-alkylation. To our delight, stirring **1** in acetone/water (v:v = 5:1) mixture led to selective cleavage of one of the TBDMS-groups affording mono-silylated analogue **6** in 92% yield. Subsequent treatment of **6** with ethyl iodide and potassium carbonate in DMF furnished *O*-alkylated aldehyde **7** in 67% yield. Subjecting aldehyde **7** into Grignard addition/DMP oxidation sequence allowed to obtain benzoyl pyridines **9a–c** in good overall yields. TBAF-promoted desilylation of **9a–b** gave a rise to pyridoxal derivatives **10a–b**. Finally, *N*-alkylation of **10a–b** with various iodo- or bromoalkanes delivered a series of *O*,*N*-bis-alkylated pyridinium salts **11a–d** in good yields ranging from 61% to 84%. The structures of representative compounds **11a–b** were

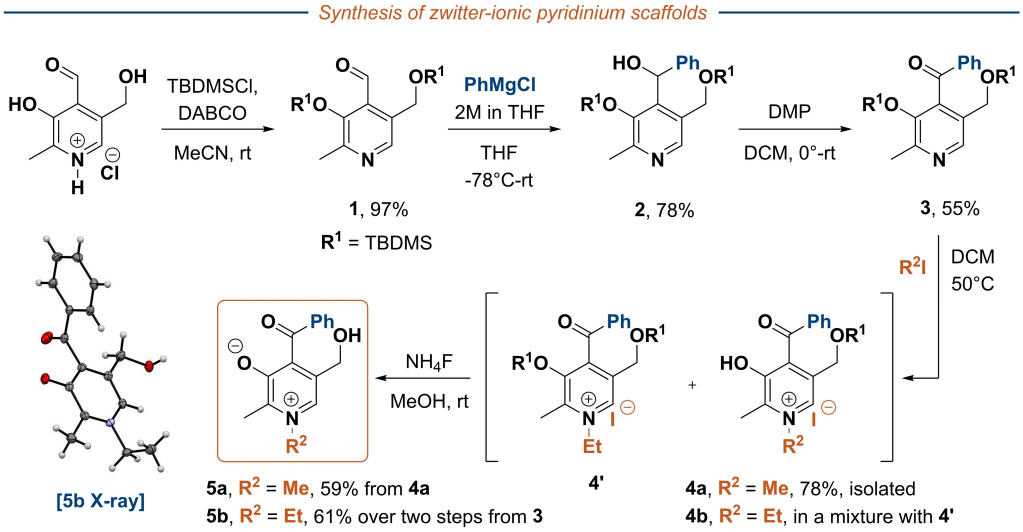

Scheme 2. Synthesis of zwitterionic pyridinium derivatives **5a–b**.

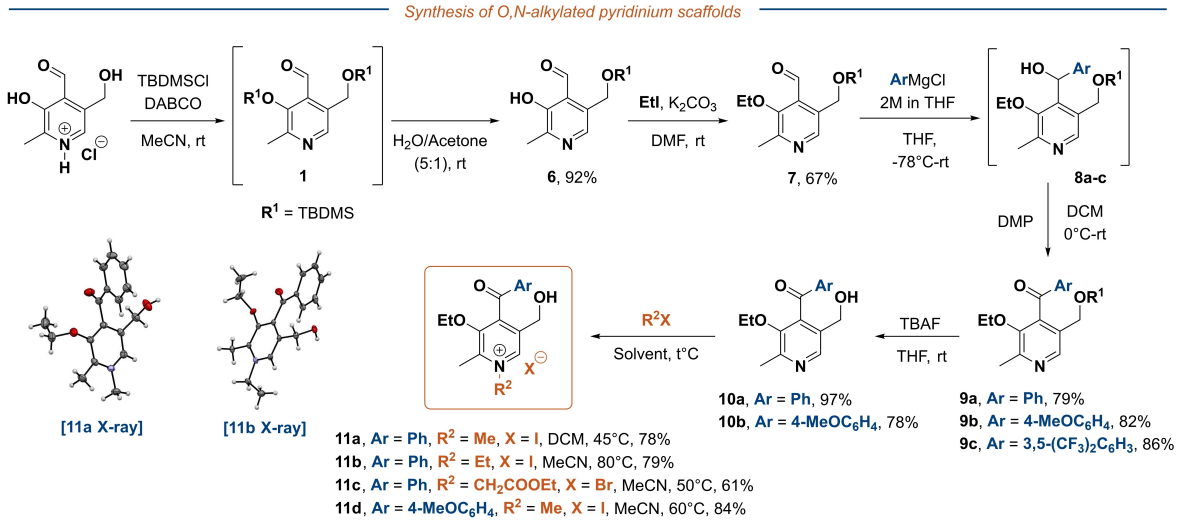

Scheme 3. Synthesis of *O,N*-bis-alkylated pyridinium salts **11a–d**; for scXRD of **11a** and **11b** iodine atoms are omitted for clarity.

resolved by single crystal XRD analysis (CCDC 2325625 and 2325624, respectively).

Interestingly, desilylation of compound **9c** bearing two electron-withdrawing trifluoromethyl groups on the aryl fragment yielded an interconvertible mixture of benzoyl pyridine **10c** and its hemiacetal **10c'** in 1:10 ratio and 79% overall yield (Scheme 4). Subjecting the obtained mixture to *N*-alkylation with iodomethane led to the exclusive formation of hemiacetal

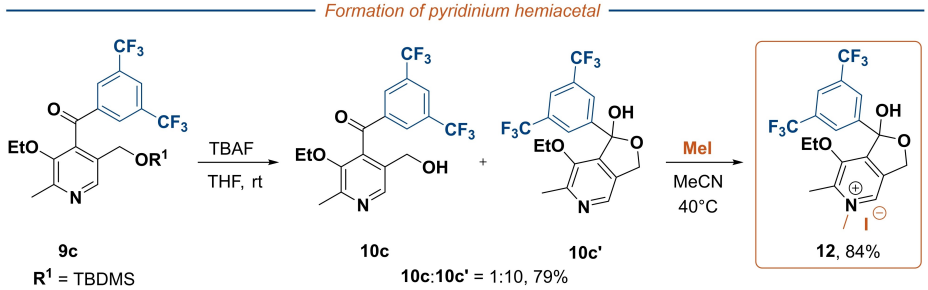

Scheme 4. Formation of hemiacetal salt **12**.

salt **12**. The ease of hemiacetal formation for this substrate can be attributed to the enhanced electrophilicity of the carbonyl group affected by the electron deficiency of the 3,5-bis(trifluoromethyl)phenyl moiety.

The synthetic pathway towards pyridinium salts **11** outlined in Scheme 3 can be slightly altered by reversing the order of two final steps of the sequence that are *N*-alkylation and silyl group removal (Scheme 5). Implementing this approach provided an alternative route to products **11a–b** as well as allowed to obtain pyridinium salt **11e** that was unattainable via the original protocol.

In our previous computational study, we also identified that an electron-withdrawing trifluoroacetyl group at the 4-position of the pyridinium framework might be beneficial for the stability of a reduced species.[24] Towards this end, we synthesized 4-trifluoroacetylpyridine **14** by the addition of trifluoromethylsilane to aldehyde **7**, followed by the TMS cleavage and DMP oxidation. This sequence provided trifluoroacetyl pyridine **14** in 40% overall yield over three steps (Scheme 6). Subsequent TBDMS removal and *N*-methylation yielded pyridinium salt **15**, which was found to favour the hemiacetal form (in analogy with **12** bearing a 3,5-bis(trifluoromethyl)phenyl group).

Finally, we attempted functionalization of the benzylic hydroxyl group of the pyridoxal core (Scheme 7). Treatment of **10a** with thionyl chloride provided straightforward access to chlorinated pyridoxal derivative **16**. AIBN-promoted reduction with tributyltin hydride produced dechlorinated benzoyl pyridine **17** in 80% yield. *N*-Alkylation of **17** with methyl iodide yielded pyridinium salt **18** lacking benzylic hydroxyl group. An attempt to perform a nucleophilic substitution of chlorine with methoxide produced an inseparable mixture of desired ketone

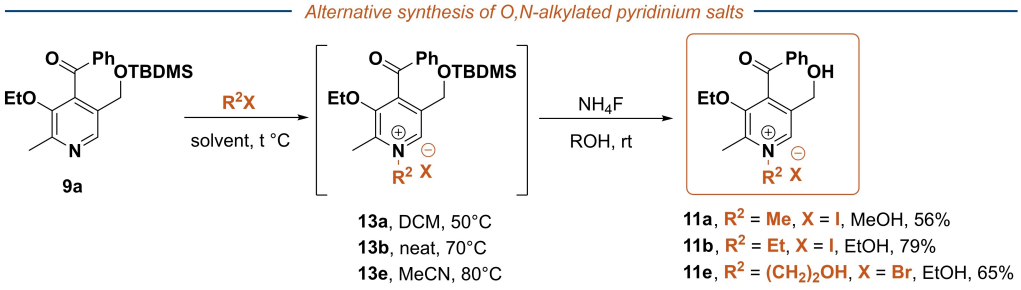

Scheme 5. Alternative alkylation/desilylation sequence for the synthesis of *O,N*-bis-alkylated pyridinium salts **11a–b, e.**

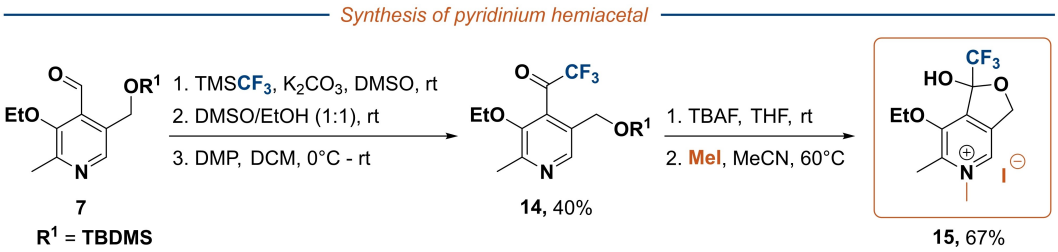

Scheme 6. Synthesis of hemiacetal salt **15**.

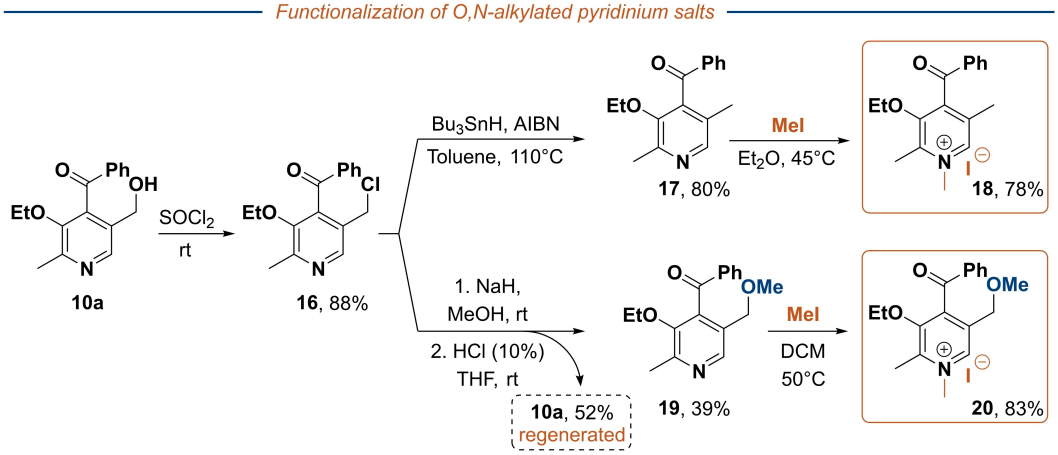

Scheme 7. Synthesis of *O,N*- bis-alkylated pyridinium salts **18** and **20** by functional group interconversion.

19 with corresponding mixed acetal. Nonetheless, treating the above mixture with 10% aq. HCl in THF delivered the desired ketone **19** along with regenerated **10a** in in 39% and 52% yields, respectively. Subsequent *N*-alkylation of **19** furnished pyridinium salt **20** featuring fully alkylated pyridoxal motif.

Next, all the generated pyridinium salts **11**, **12**, **15**, **18** and **20** were subjected to electrochemical investigations.

Electrochemical Exploration of Synthesized Pyridoxal Derivatives

The initial electrochemical tests consisted of cyclic voltammetry (CV) measurements in aqueous solutions (1 M KCl or 0.1 M NaOH). Previously, benzoyl pyridinium salts have been shown to undergo two one-electron redox processes with the individual redox steps having very close potentials (−0.83 and −0.93 V vs Ag/AgCl).[16] The first redox process was demonstrated to be reversible; however, the doubly reduced species was unstable in aqueous solutions as it reacts with water. In contrast, voltammograms of the *N*-alkylated benzoyl pyridinium salts studied herein show only one redox event taking place at potentials ranging from −0.86 V to −1.25 V. Details of the CV measurements are presented in the Supporting Information. Table 1 summarizes the voltammetry results by showing the potential of the reduction current peak (reported vs reference Ag/AgCl). The reduction peaks are chosen to assure a proper comparison between the studied compounds as some of them did not show any oxidation peak so the half wave potential cannot be calculated. The experimental reduction potentials observed in 1 M KCl (pH 7) shows a significant agreement with the predicted values from the computational protocol developed by us in the previous study (Figure 2).[24]

Substituent effects on reduction potentials (E_{red}) confirm the established downward trend for the substituents with higher electron donor strength.[26] For example, E_{red} is shifted slightly to more negative values with *N*-ethyl compared to *N*-methyl derivatives (i.e. **5a** vs. **5b**, $\Delta E_{red} = 10$ mV and **11a** vs. **11b** $\Delta E_{red} = 13$ mV, both in 0.1 M NaOH). This shift agrees with the higher electron donating strength of the longer alkyl group. In addition, compounds **11c** and **11e** with electron withdrawing substituents at the end of the *N*-alkyl pendant show a substantial potential shift to higher values compared to **11a** and **11b**. Analogously, compound **11a** bearing hydroxymethyl group in the 5-position of the pyridine core has a more positive potential ($E_{red} = -0.952$ V) compared to the 5-methyl analogue **18** ($E_{red} = -0.998$ V). As expected, moving from the zwitterionic compounds **5a** and **5b** with a deprotonated phenolate oxygen (O^-) to cationic ether derivatives **11a** and **11b**, leads to a

Table 1. Summary of cyclic voltammetry results in 1 M KCl and 0.1 M NaOH. E_{red} corresponds to the potential of the reduction peak against reference Ag/AgCl. I_{ox}/I_{red} is the ratio between the oxidation and reduction peak currents.

Compound	1 M KCl		0.1 M NaOH	
	E_{red}/V	I_{ox}/I_{red}	E_{red}/V	I_{ox}/I_{red}
5a	–[a]	–[a]	−1.242	0[b]
5b	−1.150	0[b]	−1.252	0[b]
11a	−0.802	0[b]	−0.952	0.92
11b	–[c]	–[c]	−0.965	0.91
11c	−0.671	0.22	−0.881	0.65
11d	−0.937	0.29	−0.982	0.92
11e	−0.729	0[b]	−0.866	0.85
12	–[c]	–[c]	−0.950	0.99
15	–[d]	–[d]	–[d]	–[d]
18	−0.934	0.21	−0.998	0.37
20	−0.881	0.78	−0.948	0.67

[a] The exact position of reduction current peak cannot be determined. [b] The value is zero since no oxidation process is present. [c] Cyclic voltammetry was not performed. [d] No reduction or oxidation peak is observed within the water potential window.

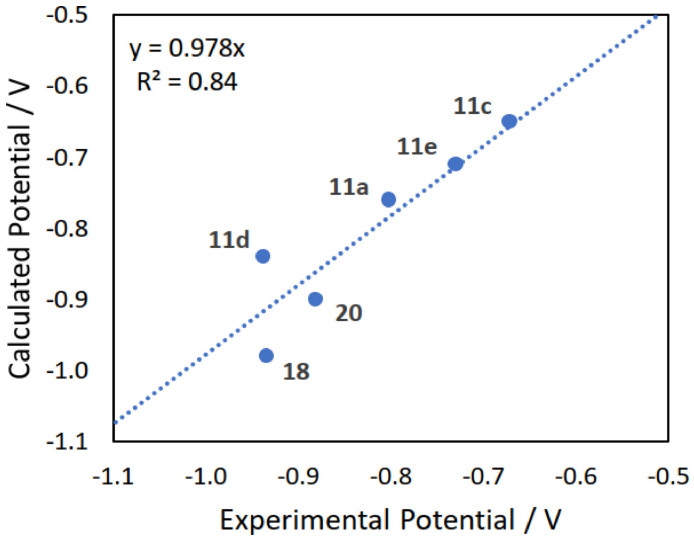

Figure 2. Comparison of the computational and experimental reduction peak potentials of the molecules tested in KCl 1 M (pH 7).

significantly more positive reduction potential (for example, for **5a**, $E_{red} = -1.242$ V *vs.* **11a**, $E_{red} = -0.952$ V) due to a weaker electron donating strength of ethoxy group compared to the O^- group as well as a higher stability of the reduced species. Introducing methoxy group in the para-position of the benzoyl fragment results in more negative reduction potential (**11e** vs. **11a**). The reduction potential of the hemiacetal derivative **12** measured in 0.1 M NaOH lies in the same range as for benzoyl pyridine derivatives **11** pointing to a possible equilibrium between the hemiacetal and keto forms, with the keto form displaying redox activity (Scheme 8).

The redox potential of hemiacetal pyridinium salt **15** appears to lie outside of the water potential window (section Electrochemical studies in SI). This could be attributed to the irreversibility of the hemiacetal formation in this case due to highly electron-withdrawing effect of the trifluoroacetyl group compared with the 3,5-bis(trifluoromethyl)benzoyl group (Scheme 8). In other words, the electron-withdrawing effect of the carbonyl group is cancelled out because of the irreversible hemiacetal formation in **15**, making the pyridinium ring more electron rich and thus the reduction potential is likely to shift significantly to more negative region.

The reduction potential of all compounds measured in both 1 M KCl and 0.1 M NaOH decreases at higher pH, suggesting a proton-coupled electron transfer (PCET) reaction, which is a well-established process in the redox chemistry of quinones.[27]

Apart from the potential of the reduction peak (vs reference Ag/AgCl), the ratio between the peak currents (oxidation/reduction) is also reported (see I_{ox}/I_{red} in Table 1). The latter is an indication of the reversibility of the system: the closer this value is to 1, the more reversible the system is. The results presented in Table 1 show that none of the molecules is reversible at neutral pH. The compound **20** shows the highest ratio between the peak currents in that media suggesting quite reversible process. However, the voltammogram exhibits a high sharp oxidation peak that indicates an adsorption of the reduced species on the working electrode followed by a stripping step during oxidation.[28] The increment of the oxidation current and peak separation at faster scan rates confirms that a weak adsorption process is occurring. That leads to a higher oxidation peak and higher current ratio; however, the process still looks poorly reversible as the current reduces significantly after multiple scans. Most of the tested compounds were found to possess a higher reversibility when tested at basic pH. The best results in 0.1 M NaOH (pH 13) were obtained for compounds **11a**, **11b**, **11d** and **12**. The latter is characterized by the highest current ratio but a very low solubility, even lower than the studied concentration of 1 mM. The compounds **18** and **20** also show low solubility not exceeding 1 mM concentration and thus we did not consider them for further studies.

Next, we investigated the stability of compounds **11a** and **11d** in a laboratory-scale flow cell. The battery studies were performed using a 5 cm^2 flow cell with graphite carbon plates and anionic exchange membrane (Selemion DSVN). The tests consisted of galvanostatic cycling using a low concentration (5–10 mM) of the studied redox material in 0.1 M NaOH on the negative side of the cell. The posolyte consisted of an excess amount of sodium ferrocyanide/ferricyanide in the same supporting electrolyte. The experiments were performed in a nitrogen filled glove box at rt. A more detailed description of the battery study is provided in the Supporting Information. The results obtained for both materials were similar: the battery was charged completely by the amount corresponding to two electrons, however just a small fraction was discharged back already in the first cycle (less than 1%). Figure 3A represents the charge and discharge profiles of compound **11a** battery test, showing the capacity accessed during the first charge -corresponding to two electrons- and the impossibility to discharge it back. These results indicate that the system undergoes a two-electron redox process and that the fully reduced form cannot be oxidized back in the studied aqueous conditions. However, switching to a more basic 2 M NaOH electrolyte with compound **11a** (Figure 3B), a significantly higher amount of the reduced species was oxidized back in the first cycle (8%). Overall, the battery was shortly cycled for five cycles before losing the rest of the capacity.

Additionally, we studied the redox process via CV analysis and electrochemical simulations. Pyridoxal derivative **11a** was selected as a model compound for these studies because of its high solubility and reversibility. Figure 4 presents the cyclic voltammograms at different scan rates of 1 mM of the active material in 0.1 M NaOH showing one high reversible redox event at −0.932 V, which differs from the two one-electron redox processes of previously studied benzoyl pyridinium salts.[15] Both the peak separation and the Randles–Ševčík equation analysis, presented in detail in the Supporting Information, suggest a two-electron redox process. We further studied and confirmed this via electrochemical simulations.

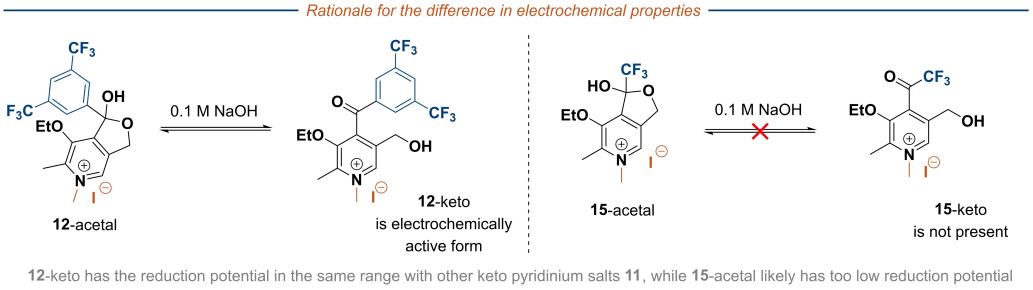

Scheme 8. Rationale for the difference in the electrochemical properties of hemiacetal salts **12** and **15**.

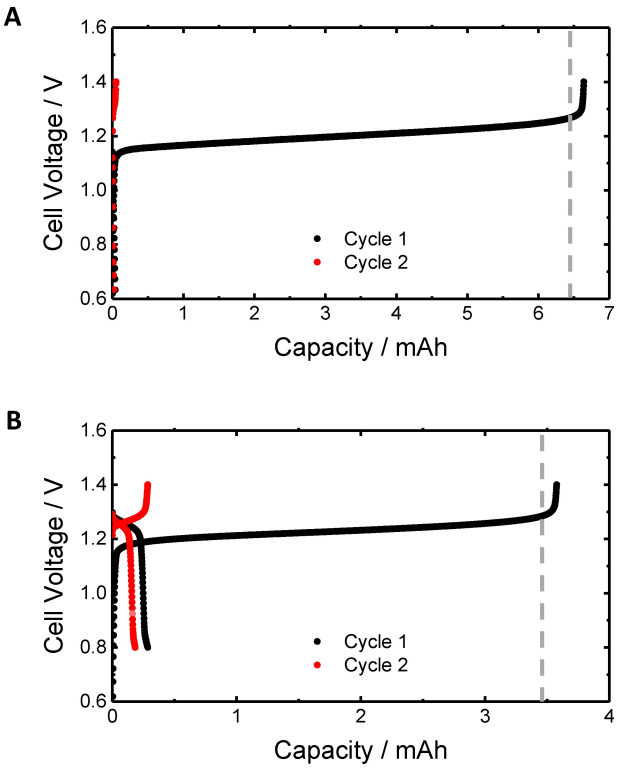

Figure 3. (A) Charge and discharge profiles of cycles 1 and 2 of flow cell with 10 mM of compound **11 a** in 0.1 M NaOH as supporting electrolyte (12 ml electrolyte). (B) Charge and discharge profiles of cycles 1 and 2 of flow cell with 5 mM of compound **11 a** in 2 M NaOH as supporting electrolyte (12 ml electrolyte). The vertical dashed line indicates the theoretical capacity expected with the assumption of 2-electron transfer.

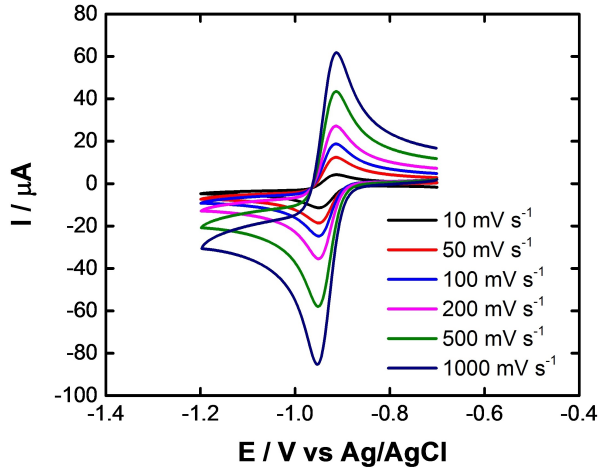

Figure 4. Cyclic voltammograms of 1 mM of compound **11 a** at different scan rates in 0.1 M NaOH. Potentials reported against reference Ag/AgCl.

First, we determined the diffusion coefficient using diffusion ordered spectroscopy (DOSY) NMR measurements and then calculated the number of electrons transferred with a model developed in COMSOL Multiphysics software (for details, see the Supporting Information). The simulations confirm that the redox process shown in the experimental voltammogram corresponds to a two-electron process (Figure 5).

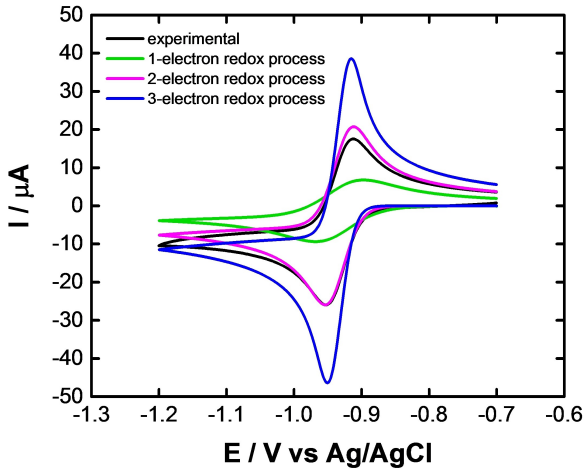

Figure 5. Experimental and simulated cyclic voltammograms of 1 mM of compound **11 a** at 100 mV s^{-1} scan rate in 0.1 M NaOH supporting electrolyte. The simulated curves correspond to 1, 2 and 3 electron redox processes. Potentials reported against reference Ag/AgCl.

Electrochemical Reduction of Pyridoxal-Based Pyridinium Salts

To gain more insight into electrochemical behavior of the synthesized *N*-alkylated benzoyl pyridinium salts, we identified and characterized the products of electrochemical reduction of representative compounds **11 a**, **18** and **20**. Conducting bulk electrolysis in an H-cell at constant potential −1.00 V in 1 M potassium chloride (phosphate buffer of pH = 8) yielded corresponding *N*-alkylated pyridoxine analogues **21 a–c** (Scheme 9). Upon completion of the reduction, alcohols **21 a–b** could be obtained in a pure form and fully characterized, while **21 c** was found to undergo partial aerobic oxidation back to **20** under the ambient conditions. Using 0.1 M sodium hydroxide (pH = 13) as the reaction media for bulk electrolysis delivered the same reduction products **21 a–c**, but the purity of the obtained samples was much lower compared to the reactions in 1 M potassium chloride. As expected on the basis of the electrochemical data (see above), two-electron reduction products **21 a–c** were obtained in the bulk electrolysis.

Alcohol **21 a** was also synthesized separately in order to provide an independent verification for the structural assignment (Scheme 10). The cyclic voltammogram of the **21 a** (both 1 M KCl and 0.1 M NaOH), presented in the Supporting information, did not show any reduction nor oxidation peak in the potential window of water, pointing at the electrochemical inactivity of this species.

Rationale for Non-Reversibility of the Process

Since a two-electron redox cycle would be potentially highly useful for energy storage, we performed a computational study to assess the thermodynamic parameters of electrochemical reduction of **11 a** into **21 a** in both neutral (pH = 7) and basic (pH = 13) media (Scheme 11). Based on the obtained results, it

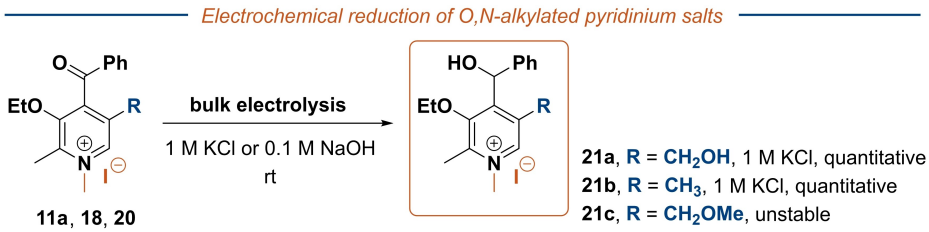

Scheme 9. Electrochemical reduction of **11 a**, **18**, **20**.

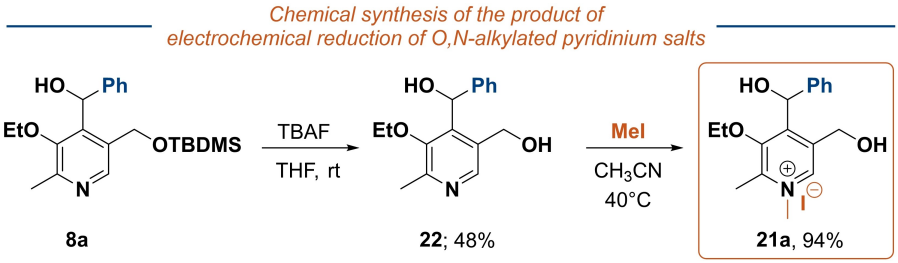

Scheme 10. Synthesis of *N*-alkylated pyridoxine analogue **21 a**.

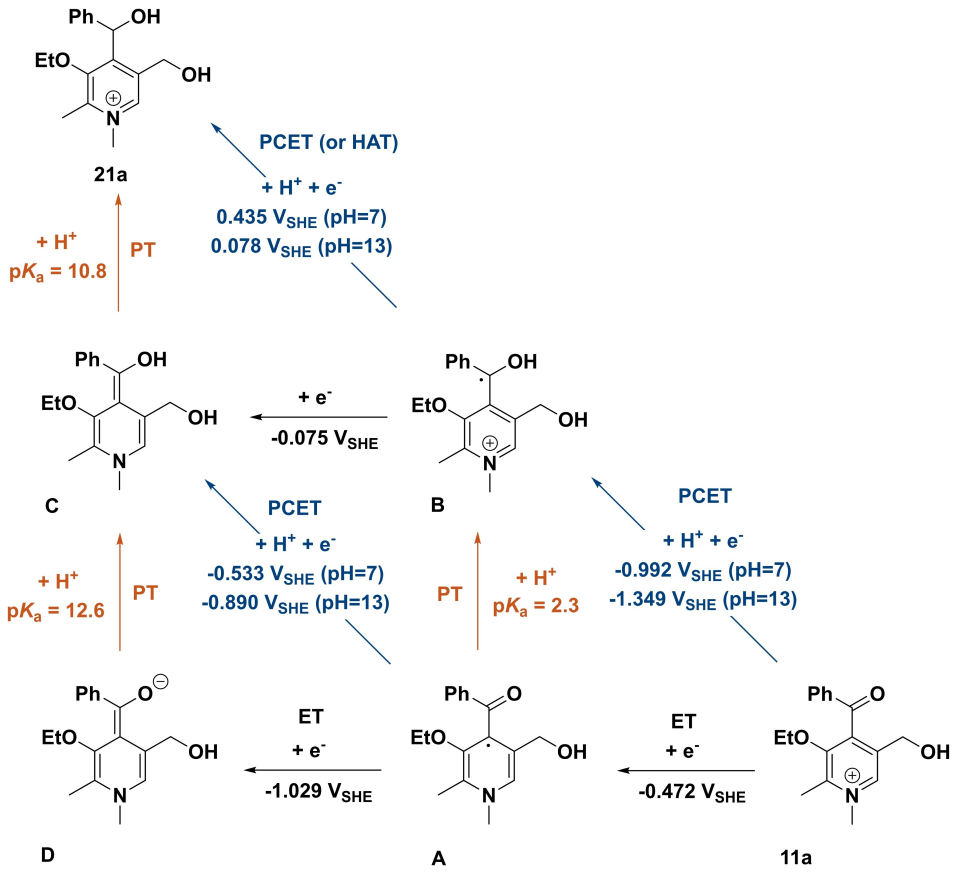

Scheme 11. Computational square representation for the reduction of compound **11 a** (for details, see the Supporting Information). The horizontal direction indicates a reduction reaction through an ET. The vertical direction indicates protonation reactions through a PT reaction. The diagonal direction indicates a reduction reaction through PCET (or hydrogen atom transfer, HAT). The reduction potentials for the PCET steps at the specific pH of 7 and 13 are computed using the Nernst equation.

can be concluded that the initial step of the entire process is the electron transfer (ET) yielding dihydropyridine radical **A**. The computed reduction potential is −0.472 V vs standard hydrogen electrode (SHE) or −0.669 V vs Ag/AgCl. An alternative pathway via radical **B** involving proton-coupled electron transfer (PCET) instead of ET would require achieving substantially more negative potential. The second reduction is likely to occur via a PCET process, yielding enol **C** from dihydropyridine radical **A**. At neutral pH, the reduction potential of this process is −0.533 V vs SHE or −0.730 V vs Ag/AgCl. Alternative pathways involving ET to intermediate **D** or proton transfer (PT) to intermediate **B** would require either more negative potential or more acidic environment, respectively. The computed ET potential for first reduction and PCET potential for second reduction have rather close values suggesting that these processes might occur simultaneously, which agrees well with experimental evidence. Computational data suggests that two processes might be separated at more basic pH through the shift of PCET potential to a more negative value. This, however, is not observed experimentally in cyclic voltammetry studies though the overall two electron reduction potential does shift to a more negative region. Finally, proton transfer (PT) of enol intermediate **C** produces *N*-alkylated pyridoxine **21 a**.

The last PT step is likely to be irreversible, which explains the absence of oxidation current peak at neutral pH in the CV curve. At pH 13, the proton transfer is slower so that **11 a** can be reduced to intermediate **C** and then oxidized back in the near electrode region during the CV measurements. However, in the laboratory scale battery experiments at the same pH, the protonation of **C** cannot be suppressed and thus the reversibility cannot be achieved as stable product **21 a** is formed. This also corroborates with the improved battery performance of compound **11 a**, attained by increasing the basicity of NaOH electrolyte from 0.1 M to 2 M (Figure 3), that underlines the impact of protonation on the stability of the doubly reduced species **C**.

According to computed p*K*a values, **21 a** has four weakly acidic sites with almost equal thermodynamic favourability for deprotonation including the two OH groups and two benzylic C–H groups (Scheme 12a). Experimentally, only the OH protons (sites 2 and 4) are rapidly exchanged with deuterons at neutral pH in D_2O (Scheme 12b). In 0.1 M NaOD in D_2O, slow H/D exchange is observed at the benzylic 2-methyl group (site 1). Even prolonged reaction times did not lead to H/D exchange at site 3, the second benzylic C–H. The electrochemical oxidation of benzylic alcohols is known to be challenging[8,29] since it requires a kinetically slow C–H deprotonation or hydrogen atom transfer/PCET step.[30] Thus, once the two-electron reduction product **21 a** is formed, it cannot be deprotonated into the intermediate **C** due to either thermodynamic or kinetic[31] reasons and therefore the subsequent oxidation back into the ketone **11 a** cannot be realized.

Although the computationally predicted reduction potentials for the vitamin B_6-based anolytes were found to be quite reliable, the prediction of irreversibility of the reduction processes in anolyte design, especially in aqueous media, is more challenging. In this study, even candidates that appeared to give a reversible redox cycle in CV tests, such as **11 a**, turned out to exhibit irreversible 2-electron-2 proton reduction of the ketone to the benzylic alcohol under laboratory-scale electrolysis tests. In recent molecular designs involving pyridinium-based anolytes, the ketone group has been replaced by other functionalities, such as malononitriles[32] or aryl groups[33] These designs, however, are generally suited for organic solvents instead of aqueous solutions.

Conclusions

In summary, we have outlined the synthetic framework for accessing diverse vitamin B_6-based redox-active benzoyl pyridinium salts starting from the readily available pyridoxal hydrochloride. Altering the structure and electronic properties

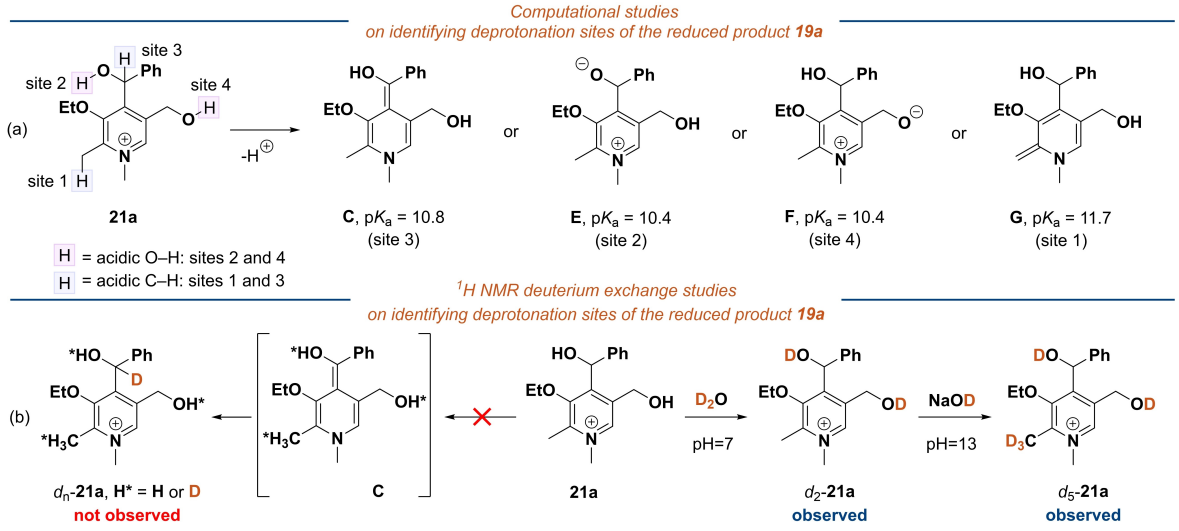

Scheme 12. Studies on identifying deprotonation sites of the reduced product **21 a**.

of the pyridoxal core allowed identifying compounds that showed promise in cyclic voltammetry in basic aqueous media. However, the results obtained with the laboratory-scale FB were negative. Consequently, we have focused on understanding the electrochemical behaviour of these pyridoxal-based scaffolds. In particular, using CV analysis and electrochemical simulations we have shown that the redox wave observed in the experimental voltammograms of our compounds corresponds to a two-electron process. By performing bulk electrolysis of several representative compounds we were able to isolate and characterize the reduction products incorporating the secondary alcohol moiety resulting from 2-electron reduction of the ketone carbonyl. Based on the experimental evidence and computational data, the overall transformation follows a ET/PCET/PT sequence, with the first two steps occurring at the same reduction potential and the final protonation step being irreversible. Overall, the integrated approach, including bulk electrochemistry tests, turned out to be a highly reliable workflow for assessing the viability of compounds for electrochemical applications in aqueous solutions. Furthermore, the results obtained by us could be useful for designing next generation redox active pyridoxal/pyridinium ketone derivatives suitable for FB technology. In particular, additional efforts can be directed to introducing scaffold changes that can either suppress the late-stage protonation or facilitate the separation of ET and PCET towards reversible cycling at the potential of first electron transfer.

Experimental Section

General Details

Unless otherwise specified, the following general procedures were used in all reactions. Acetonitrile, THF and CH_2Cl_2 were obtained by passing deoxygenated solvents through activated alumina columns (MBraun SPS-800 Series solvent purification system). Other solvents and reagents were used as obtained from supplier, unless otherwise noted. Analytical TLC was performed using Merck silica gel F254 (230–400 mesh) plates and analyzed by UV light. For silica gel chromatography, the flash chromatography technique was used, with Merck silica gel 60 (230–400 mesh) and p.a. grade solvents unless otherwise noted. The ^{1}H NMR and ^{13}C NMR spectra were recorded in either $CDCl_3$, $(CD_3)_2SO$ or CD_3OD on Bruker Avance III 300 MHz and Bruker Avance III 500 MHz spectrometers. The chemical shifts are reported in ppm relative to $CDCl_3$, δ 7.26 ppm and δ 77.16 ppm; $(CD_3)_2SO$, δ 2.50 ppm and δ 39.52 ppm; MeOD δ 3.31 and δ 49.00 ppm for ^{1}H NMR and ^{13}C NMR spectra respectively. Melting points (mp) were determined in open capillaries using melting point apparatus Stuart Scientific SMP3. IR spectra were recorded on a FT-IR spectrometer Bruker Alpha. High resolution mass spectrometric data were measured using Agilent 6560 ESI-IM-QTOF mass spectrometer equipped with AJS ESI ion source.

5-(((*tert*-Butyldimethylsilyl)Oxy)Methyl)-3-Hydroxy-2-Methylisonicotinaldehyde (6)

Pyridoxal hydrochloride (12.2 g, 60 mmol) was placed into a 1000 mL screw-cap vessel and dry acetonitrile (600 mL) was added *via* cannula under argon atmosphere. Then, 1,4-diazabicyclo[2.2.2]octane (DABCO, 40.4 g, 360 mmol) and *tert*-butyldimethylsilyl chloride (22.6 g, 150 mmol) were added. The reaction mixture was covered with aluminium foil and stirred for 72 h at rt. The reaction mixture was filtered and the filtrate was concentrated in a rotary evaporator. The residue was diluted with ethyl acetate (300 mL), transferred to a separation funnel and then washed with sat. aq. solution of $NaHCO_3$ (1×500 mL) and brine (1×500 mL). The organic layer was dried over Na_2SO_4, filtered, and concentrated under reduced pressure. The residue was dried in a high vacuum line at 40–50 °C for 48 h to remove all silicon containing impurities. Then, acetone/water mixture (80/16 mL) was added to the resulting crude product **1**, and the mixture was left stirring for 24 h at rt until the completion of the reaction as indicated by a TLC analysis. The resulting mixture was diluted with ethyl acetate (200 mL), transferred to a separation funnel and then washed with brine (1×300 mL). The organic layer was dried over Na_2SO_4, filtered, and concentrated under reduced pressure. The residue was dried in a high vacuum line at 40–50 °C for 48 h to remove all silicon containing impurities, yielding **6** as a yellow solid (16.5 g, 97 %). The silylation reaction was performed several times and the isolated yields were in the range of 92–97 %.

Note: Due to the sensitivity of the reaction to adventitious moisture, it is strongly recommended to carry out the reaction in a closed screw-cap vessel to obtain the product with high chemoselectivity. Checking the TLC during the reaction is not recommended!

mp. 72–75 °C; **IR** (neat, ATR) ν_{max} 2954, 2929, 2856, 1671, 1059, 834 cm^{-1}; **^{1}H NMR** (300 MHz, $CDCl_3$) δ 10.51 (s, 1H), 8.04 (s, 1H), 4.94 (s, 2H), 2.56 (s, 3H), 0.88 (s, 9H), 0.09 (s, 6H); **^{13}C NMR** (75 MHz, $CDCl_3$) δ 197.5, 153.9, 151.9, 138.3, 132.7, 120.3, 60.6, 25.7, 18.7, 18.1, −5.2; **HRMS** (ESI^+): m/z $[M+H]^+$ calcd for $[C_{14}H_{24}NO_3Si]^+$ 282.1519, found 282.1521.

5-(((*tert*-Butyldimethylsilyl)Ooxy)Methyl)-3-Ethoxy-2-Methylisonicotinaldehyde (7)

Aldehyde **6** (15.9 g, 56.4 mmol) was placed into 250 mL round-bottom flask and dissolved in dry DMF (190 mL) under argon atmosphere at rt. Then, potassium carbonate (9.34 g, 67.7 mmol) was added, and the mixture was stirred for 15 minutes followed by a dropwise addition of diethyl sulphate (8.87 mL, 67.7 mmol). The reaction mixture was then stirred for 4 h at rt. The resulting mixture was filtered and the filtrate was diluted with diethyl ether (200 mL), transferred to a separation funnel and then washed with water (2×400 mL). The combined aqueous layers were extracted with diethyl ether (200 mL). The combined organic layers were dried over Na_2SO_4, filtered, and concentrated under reduced pressure. Column chromatography on silica with hexane/ethyl acetate (85 : 15) mixture as the eluent yielded **7** as a pale yellow oil (10.5 g, 60 %).

IR (neat, ATR) ν_{max} 2953, 2929, 2856, 1693, 1110, 834 cm^{-1}; **^{1}H NMR** (300 MHz, $CDCl_3$) δ 10.54 (s, 1H), 8.71 (s, 1H), 5.21–4.81 (m, 2H), 4.01 (q, J = 7.0 Hz, 2H), 2.58 (s, 3H), 1.45 (t, J = 7.0 Hz, 3H), 0.94 (s, 9H), 0.11 (s, 6H).; **^{13}C NMR** (75 MHz, $CDCl_3$) δ 192.5, 154.8, 153.4, 143.5, 134.9, 131.2, 72.3, 61.3, 26.0, 19.2, 18.4, 15.5, −5.2; **HRMS** (ESI^+): m/z $[M+H]^+$ calcd for $[C_{16}H_{27}NO_3Si]^+$ 310.1832, found 310.1852.

(5-(((*tert*-Butyldimethylsilyl)oxy)Methyl)-3-Ethoxy-2-Methylpyridin-4-Yl)(Phenyl)Methanol (8 a)

Aldehyde **7** (10.5 g, 33.9 mmol) was placed into a 500 mL round-bottom flask and dissolved in dry THF (217 mL) under argon atmosphere. The resulting mixture was cooled to −78 °C using acetone bath, followed by a dropwise addition of phenyl magnesium chloride (2.0 M solution in THF, 67.7 mL) via syringe. The resulting solution was slowly warmed up to rt and stirred for

16 h. The reaction mixture was quenched with sat. aq. solution of ammonium chloride (150 mL) and concentrated to remove the main part of THF. The remaining volume was extracted with ethyl acetate (1×150 mL). The organic layer was washed with brine (1×150 mL), dried over Na_2SO_4, filtered, and concentrated under reduced pressure. The residue was triturated with MTBE and the product was collected by filtration, yielding **8a** as a white powder (9.14 g, 71%).

mp. 180–183 °C; **IR** (neat, ATR) ν_{max} 3067, 2956, 2929, 2857, 1045, 837, 777 cm^{-1}; **^{1}H NMR** (300 MHz, $CDCl_3$) δ 8.13 (s, 1H), 7.37–7.18 (m, 5H), 6.30 (d, J=10.7 Hz, 1H), 5.05 (d, J=10.8 Hz, 1H), 4.33 (d, J=1.2 Hz, 2H), 3.91 (dq, J=9.1, 7.0 Hz, 1H), 3.76 (dq, J=9.2, 7.0 Hz, 1H), 2.57 (s, 3H), 1.34 (t, J=7.0 Hz, 3H), 0.87 (s, 8H), 0.04 (d, J=10.1 Hz, 6H); **^{13}C NMR** (75 MHz, $CDCl_3$) δ 153.8, 152.0, 145.2, 144.6, 143.3, 132.2, 128.2, 127.1, 125.5, 70.3, 68.5, 62.0, 25.9, 19.9, 18.3, 15.6, −5.2, −5.2; **HRMS** (ESI^+): m/z $[M+H]^+$ calcd for $[C_{22}H_{33}NO_3Si]^+$ 388.2302, found 388.2327.

(5-(((*tert*-Butyldimethylsilyl)Oxy)Methyl)-3-Ethoxy-2-Methylpyridin-4-Yl)(Phenyl)Methanone (9a)

Alcohol **8a** (9.32 g, 24.04 mmol) was placed into a 500 mL round-bottom flask and dissolved in dry dichloromethane (220 mL) under argon atmosphere. The mixture was cooled to 0 °C. Dess–Martin periodinane (DMP) (15.3 g, 36.06 mmol) was added in small portions and the resulting mixture was stirred for 16 h. Sat. aq. $NaHCO_3$ solution (1×300 mL) was then added, the layers were separated, and the organic layer was washed with saturated $Na_2S_2O_3$ (1×300 mL) and brine (1×300 mL). The combined organic layers were dried over Na_2SO_4, filtered, and concentrated under reduced pressure. Column chromatography on silica gel with hexanes/ethyl acetate (80:20) mixture as the eluent yielded **9a** as a pale brown amorphous material (8.75 g, 94%).

Alternative One-Pot Grignard Addition/Oxidation Pathway

Phenylmagnesium bromide (1 M in THF, 17.8 mL) was added over a period of 30 min to a stirred solution of aldehyde **7** (5 g, 16.16 mmol) in 100 mL of dry THF at 0 °C. The completion of the reaction was monitored by TLC. The reaction was then quenched with saturated solution of ammonium chloride (30 mL) followed by addition of ethyl acetate (50 mL). The aqueous layer was separated and extracted with ethyl acetate (2×50 mL), and the combined organic layers were washed with brine (50 mL), dried over Na_2SO_4, filtered, and concentrated under reduced pressure yielding crude **8a** (6.0 g) which was used in the next step without further purification.

Crude **8a** (6 g, 15.5 mmol) was dissolved with dry dichloromethane (100 mL) at 0 °C and Dess-Martin periodinane (7.22 g, 17.04 mmol) was added in three portions at a regular interval of 10 minutes. After 2 h, sat. aq. solution of $NaHCO_3$ (100 mL) was added, and the reaction mixture was allowed to stir for 1 h. The aqueous layer was separated and extracted with dichloromethane (2×100 mL). The combined organic layers were dried over Na_2SO_4, filtered, and concentrated under reduced pressure. Column chromatography on silica with hexane/ethyl acetate (80:20) mixture as the eluent gave **9a** as a pale brown amorphous material (4.7 g, 79% over two steps).

IR (neat, ATR) ν_{max} 2949, 2927, 2854, 1670, 1060, 834 cm^{-1}; **^{1}H NMR** (300 MHz, $CDCl_3$) δ 8.36 (s, 1H), 7.85–7.70 (m, 2H), 7.61-7.51 (m, 1H), 7.49–7.37 (m, 2H), 4.58 (s, 2H), 3.78 (q, J=7.0 Hz, 2H), 2.53 (s, 3H), 1.08 (t, J=7.0 Hz, 3H), 0.73 (s, 9H), −0.15 (s, 6H); **^{13}C NMR** (75 MHz, $CDCl_3$) δ 195.6, 152.7, 149.9, 143.3, 139.5, 136.8, 133.9, 132.5, 129.5, 128.7, 70.7, 60.7, 25.8, 19.5, 18.3, 15.4, −5.7; **HRMS** (ESI^+): m/z $[M+H]^+$ calcd for $[C_{22}H_{31}NO_3Si]^+$ 386.2145, found 386.2154.

(3-Ethoxy-5-(Hydroxymethyl)-2-Methylpyridin-4-Yl)(Phenyl)Methanone (10a)

Ketone **9a** (8.75 g, 22.7 mmol) was placed into a 500 mL round-bottom flask and dissolved in dry tetrahydrofuran (220 mL) under argon atmosphere at rt. Then, tetra-*n*-butylammonium fluoride hydrate (TBAF, 8.9 g, 34.0 mmol) was added, and the resulting mixture was stirred for 3 h. The reaction mixture was diluted with ethyl acetate (250 mL) and the organic layer was washed with water (1×500 mL) and brine (1×500 mL). The organic layer was dried over Na_2SO_4, filtered, and concentrated under reduced pressure. Column chromatography with gradient hexanes/ethyl acetate (95:25→5:75) as the eluent yielded **10a** as a pale brown glue-like material (6.0 g, 97%).

IR (neat, ATR) ν_{max} 3207, 2987, 2928, 2892, 1670, 1275, 1024, 689 cm^{-1}; **^{1}H NMR** (300 MHz, $CDCl_3$) δ 8.36 (s, 1H), 7.86-7.72 (m, 2H), 7.66–7.55 (m, 1H), 7.46 (dd, J=8.3, 7.1 Hz, 2H), 4.50 (s, 2H), 3.78 (q, J=7.0 Hz, 2H), 2.77 (bs, 1H), 2.53 (s, 3H), 1.06 (t, J=7.0 Hz, 3H); **^{13}C NMR** (75 MHz, $CDCl_3$) δ 196.6, 153.4, 150.0, 144.4, 139.7, 136.6, 134.3, 132.6, 129.6, 128.9, 70.8, 60.5, 19.6, 15.4; **HRMS** (ESI^+): m/z $[M+H]^+$ calcd for $[C_{16}H_{18}NO_3]^+$ 272.1208, found 272.1289.

4-Benzoyl-3-Ethoxy-5-(Hydroxymethyl)-1,2-Dimethylpyridin-1-Ium Iodide (11a)

Ketone **10a** (0.32 g, 1.19 mmol) was placed into a screw-cap vial followed by addition of dry dichloromethane (4 mL) under argon atmosphere. Then, methyl iodide (0.65 mL, 11.9 mmol) was added, and the reaction was stirred for 24 h at 45 °C. The reaction mixture was diluted with diethyl ether (10 mL) to precipitate the product, and the precipitate was collected by filtration to give **11a** as a pale grey crystalline material (0.39 g, 78%).

Alternative Synthesis Via Reversed Alkylation/Desilylation Sequence

Ketone **9a** (0.65 g, 1.8 mmol) was placed into a 20 ml screw-cap vial and dissolved in dry dichloromethane (5.0 mL) under argon atmosphere. Then, iodomethane (0.98 mL, 18 mmol) was added, and the reaction was left stirring for 48 h at 50 °C covered with an aluminium foil. The reaction mixture was diluted with chloroform (30 mL) and washed with brine (1×40 mL). The aqueous layer was extracted with chloroform (30 mL). The combined organic layers were dried over Na_2SO_4, filtered, and concentrated under reduced pressure to give crude **13a** as a brownish powder (0.87 g, 91%). Then, a portion of crude silylated pyridinium salt **13a** (0.35 g, 0.66 mmol) was placed to a plastic screw-cap vial followed by addition of methanol (14 mL). Then, ammonium fluoride (0.23 g, 6.6 mmol) was added and the reaction mixture was stirred for 5 h at rt covered with an aluminium foil. The mixture was concentrated under reduced pressure. The resulting residue was extracted with chloroform (5×10 mL) and the remaining inorganic salts were filtered off through a cotton/sand plug. The organic filtrate was concentrated under reduced pressure. The crude product thus obtained was recrystallized from a minimum amount of water and washed with cold water (3×0.3 mL) and diethyl ether (3×3 mL), yielding **11a** as a pale grey crystalline material (0.15 g, 56%).

mp. 194–196 °C; **Anal. Calcd** for $C_{17}H_{20}INO_3$: C 49.41%, H 4.88%, N 3.39%; Found: C 49.12%, H 5.18%, N 3.62%; **IR** (neat, ATR) ν_{max} 3303, 3013, 2990, 2906, 1671, 1282, 1021, 710 cm^{-1}; **^{1}H NMR** (300 MHz, Methanol-d_4) δ 8.81 (s, 1H), 7.99–7.82 (m, 2H), 7.79–7.66

(m, 1H), 7.63–7.49 (m, 2H), 4.58 (s, 2H), 4.38 (s, 3H), 4.10–3.84 (m, 2H), 2.80 (s, 3H), 1.15 (t, J = 7.0 Hz, 3H); **^{13}C NMR** (75 MHz, Methanol-d_4) δ 193.18, 154.45, 153.71, 147.59, 141.45, 139.42, 136.58, 136.33, 130.66, 130.34, 74.08, 59.31, 47.81, 15.38, 14.88; **HRMS** (ESI$^+$): m/z $[M]^+$ calcd for $[C_{17}H_{20}NO_3]^+$ 286.1443, found 286.1431.

Cyclic Voltammetry Measurements

We performed the cyclic voltammetry tests with Biologic Potentiostat SP-240 (or SP-150) or Gamry Reference [600]+ potentiostat. For all CV tests, glassy carbon (3.0 mm diameter), Ag/AgCl (3 M KCl solution), and platinum wire were used as the working electrode, reference electrode, and counter electrode; respectively. Prior to each test, we polished the glassy carbon with 1 μm alumina and rinsed with DI water. The solution was degassed by bubbling nitrogen for 10 minutes before each experiment. The concentration of the studied material was 1 mM in 10 ml of the supporting electrolyte. The resistance of the solution was measured using potentiometric electrochemical impedance spectroscopy (PEIS). All the potentials are reported against Ag/AgCl reference.

Battery Tests

The battery experiments were performed using a 5 cm^2 flow cell with graphite carbon plates. The electrodes were SGL carbon felts 4,6 mm from SIGRACELL (thermally activated) which were sonicated in DI water for 10 minutes before assembling the battery. Anionic exchange membrane (AEM) Selemion DSVN from AGC was used as a membrane. The flow rate was 50 ml min^{-1} using a peristaltic pump Baoding Chuangrui and the tubing was Masterflex C-Flex. The cycling was performed galvanostatically using a cycler LANHE Battery Testing System G340A and all the tests were performed inside a nitrogen-filled Glovebox (MBRAUN) at 30 °C.

The posolyte consisted of a solution of sodium ferrocyanide/ferricyanide in the same supporting electrolyte, taken in an excess amount corresponding to a two-electron reduction of the tested negolyte in order to ensure that the latter is the limiting side.

Supporting Information

Supporting Information

Full experimental procedures, product characterization data, copies of NMR spectra, and complete details of electrochemical and computational studies (PDF).[34,35,36,37,38,39,40,41,42,43,44,45,46,47,48,49,50,51,52]

Deposition Number(s) 2325623 (for **5b**), 2325625 (for **11a**), 2325624 (for **11b**) contain the supplementary crystallographic data for this paper. These data are provided free of charge by the joint Cambridge Crystallographic Data Centre and Fachinformationszentrum Karlsruhe Access Structures service.

Acknowledgements

This project has received funding from the European Union's Horizon2020 Research and Innovation programme under grant agreement No 875565 (Project CompBat). Support from Research Council Finland (projects 322899 and 348328 – via European Union – NextGenerationEU instrument – to P. M. P.) and 346895 (to A. N.), as well as project DIGIPOWER (Technology Industries of Finland Centennial Foundation and Jane & Aatos Erkko Foundation) is also acknowledged. A. B. thanks the Chemistry Department of University of Jyväskylä for funding, Prof. Kari Rissanen for training in crystallography and assistance in measurement of the structures **5b** and **11a**. The organizing committee of Zürich Summer School of Crystallography is thanked for assistance in measuring and solving the structure **11b** (in particular Dr. Michael D. Wörle, Dr. Nils Trapp and Dr. Farzaneh Fadaei-Tirani). We also thank Dr. Elina Kalenius and Dr. Anniina Kiesilä for assistance with mass spectrometry, Dr. Esa Haapaniemi for NMR assistance, and Doc. Elina Sievänen (all at Jyväskylä) for assistance with CompBat project management. P. P. gratefully acknowledges the Academy Research Fellow funding (grant no. 315739, 343791, 320071 and 343794) and BioFlow project (grant no. 343493) from Research Council Finland, and European Research Council through a Starting grant (agreement no. 950038).

Conflict of Interests

The authors declare no conflict of interest.

Data Availability Statement

The data that support the findings of this study are available in the supplementary material of this article.

Keywords: pyridinium ions · pyridoxal · vitamin B6 · electrochemistry · flow batteries

[1] a) M. Z. Jacobson, M. A. Delucchi, Z. A. F. Bauer, S. C. Goodman, W. E. Chapman, M. A. Cameron, C. Bozonnat, L. Chobadi, H. A. Clonts, P. Enevoldsen, J. R. Erwin, S. N. Fobi, O. K. Goldstrom, E. M. Hennessy, J. Liu, J. Lo, C. B. Meyer, S. B. Morris, K. R. Moy, P. L. O'Neill, I. Petkov, S. Redfern, R. Schucker, M. A. Sontag, J. Wang, E. Weiner, A. S. Yachanin, *Joule* **2017**, *1*, 108–121; b) P. Das, J. Mathur, R. Bhakar, A. Kanudia, *Energy Strategy Rev.* **2018**, *22*, 1–15.
[2] G. L. Soloveichik, *Chem. Rev.* **2015**, *115*, 11533–11558.
[3] K. Lourenssen, J. Williams, F. Ahmadpour, R. Clemmer, S. Tasnim, *J. Energy Storage* **2019**, *25*, 100844.
[4] D. Larcher, J.-M. Tarascon, *Nat. Chem.* **2015**, *7*, 19.
[5] a) Y. Liu, Q. Chen, P. Sun, Y. Li, Z. Yang, T. Xu, *Mater. Today Energy* **2021**, *20*, 100634; b) Z. Li, T. Jiang, M. Ali, C. Wu, W. Chen, *Energy Storage Mater.* **2022**, *50*, 105–138.
[6] a) B. Huskinson, M. P. Marshak, C. Suh, S. Er, M. R. Gerhardt, C. J. Galvin, X. Chen, A. Aspuru-Guzik, R. G. Gordon, M. J. Aziz, *Nature* **2014**, *505*, 195–198; b) B. Hu, J. Luo, M. Hu, B. Yuan, T. L. Liu, *Angew. Chem. Int. Ed.* **2019**, *58*, 16629–16636; c) E. F. Kerr, Z. Tang, T. Y. George, S. Jin, E. M. Fell, K. Amini, Y. Jing, M. Wu, R. G. Gordon, M. J. Aziz, *ACS Energy Lett.* **2022**, *8*, 600–607.
[7] a) Y. Liu, M.-A. Goulet, L. Tong, Y. Liu, Y. Ji, L. Wu, R. G. Gordon, M. J. Aziz, Z. Yang, T. Xu, *Chem* **2019**, *5*, 1861–1870; b) B. Hu, M. Hu, J. Luo, T. L. Liu, *Adv. Energy Mater.* **2021**, *12*, 2102577; c) M. Pan, L. Gao, J. Liang, P. Zhang, S. Lu, Y. Lu, J. Ma, Z. Jin, *Adv. Energy Mater.* **2022**, *12*, 2103478.
[8] R. Feng, X. Zhang, V. Murugesan, A. Hollas, Y. Chen, Y. Shao, E. Walter, N. P. N. Wellala, L. Yan, K. M. Rosso, W. Wang, *Science* **2021**, *372*, 836–840.
[9] A. Orita, M. G. Verde, M. Sakai, Y. S. Meng, *Nat. Commun.* **2016**, *7*, 13230.
[10] A. Ramar, F.-M. Wang, R. Foeng, R. Hsing, *J. Power Sources* **2023**, *558*, 232611.
[11] S. Sowmiah, J. M. S. S. Esperança, L. P. N. Rebelo, C. A. M. Afonso, *Org. Chem. Front.* **2018**, *5*, 453–493.

[12] S. L. Rössler, B. J. Jelier, E. Magnier, G. Dagousset, E. M. Carreira, A. Togni, *Angew. Chem. Int. Ed.* **2020**, *59*, 9264–9280.
[13] a) T. Liu, X. Wei, Z. Nie, V. Sprenkle, W. Wang, *Adv. Energy Mater.* **2015**, *6*, 1501449; b) S. Jin, E. M. Fell, L. Vina-Lopez, Y. Jing, P. W. Michalak, R. G. Gordon, M. J. Aziz, *Adv. Energy Mater.* **2020**, *10*, 2000100; c) M. Hu, W. Wu, J. Luo, T. L. Liu, *Adv. Energy Mater.* **2022**, *12*, 2202085.
[14] J. Huang, Z. Yang, V. Murugesan, E. Walter, A. Hollas, B. Pan, R. S. Assary, I. A. Shkrob, X. Wei, Z. Zhang, *ACS Energy Lett.* **2018**, *3*, 2533–2538.
[15] a) N. Leventis, I. A. Elder, X. Gao, E. W. Bohannan, C. Sotiriou-Leventis, A. M. Rawashdeh, T. J. Overschmidt, K. R. Gaston, *J. Phys. Chem. B* **2001**, *105* (17), 3663–3674; b) C. S. Sevov, R. E. M. Brooner, E. Chénard, R. S. Assary, J. S. Moore, J. Rodríguez-López, M. S. Sanford, *J. Am. Chem. Soc.* **2015**, *137*, 14465–14472; c) C. S. Sevov, D. P. Hickey, M. E. Cook, S. G. Robinson, S. Barnett, S. D. Minteer, M. S. Sigman, M. S. Sanford, *J. Am. Chem. Soc.* **2017**, *139*, 2924–2927; d) K. H. Hendriks, C. S. Sevov, M. E. Cook, M. S. Sanford, *ACS Energy Lett.* **2017**, *2*, 2430–2435.
[16] C. S. Sevov, K. H. Hendriks, M. S. Sanford, *J. Phys. Chem. C* **2017**, *121*, 24376–24380.
[17] P. W. Antoni, T. Bruckhoff, M. M. Hansmann, *J. Am. Chem. Soc.* **2019**, *141*, 9701–9711.
[18] H. Hellmann, S. Mooney, *Molecules* **2010**, *15*, 442–459.
[19] https://fi.espacenet.com/publicationDetails/biblio?II=0&ND=3&adjacent=true&locale=fi FI&FT=D&date=19980616&CC=US&NR=5766894 A&KC=A.
[20] For the comprehensive overview, see: Y. G. Shtyrlin, A. S. Petukhov, A. D. Strelnik, N. V. Shtyrlin, A. G. Iksanova, M. V. Pugachev, R. S. Pavelyev, M. S. Dzyurkevich, M. R. Garipov, K. V. Balakin, *Russ. Chem. Bull.* **2019**, *68*, 911–945.
[21] For examples of side chain functionalization, see: a) W. Korytnyk, P. Burton, *J. Med. Chem.* **1970**, *13*, 187–191; b) J. A. Yazarians, B. L. Jiménez, G. R. Boyce, *Tetrahedron Lett.* **2017**, *58*, 2258–2260.
[22] For the synthesis of vitamin B_6 derived Schiff base complexes, see: S. Gupta, *Rev. Inorg. Chem.* **2021**, *42*, 161–177.
[23] For the applications of vitamin B_6 in heterocyclic synthesis, see: a) F. Fringuelli, G. Brufola, O. Piermatti, F. Pizzo, *Heterocycles* **1997**, *45*, 1715; b) V. Y. Sosnovskikh, V. Y. Korotaev, A. Y. Barkov, A. A. Sokovnina, M. I. Kodess, *J. Fluorine Chem.* **2012**, *141*, 58–63; c) L. Pizzuti, I. Casadia, T. O. Daher, S. Moura, D. F. Back, E. Faoro, C. S. Schwalm, G. A. Casagrande, G. C. Paveglio, *Synthesis* **2020**, *53*, 365–370.
[24] A. Hamza, F. B. Németh, Á. Madarász, A. Nechaev, P. Pihko, P. Peljo, I. Pápai, *Chem. Eur. J.* **2023**, *29*, e202300996.
[25] M. Chatenet, B. G. Pollet, D. R. Dekel, F. Dionigi, J. Deseure, P. Millet, R. D. Braatz, M. Z. Bazant, M. Eikerling, I. Staffell, P. Balcombe, Y. Shao-Horn, H. Schäfer, *Chem. Soc. Rev.* **2022**, *51*, 4583–4762.
[26] K. M. Pelzer, L. Cheng, L. A. Curtiss, *J. Phys. Chem. C* **2017**, *121*, 237–245.
[27] a) C. Costentin, *Chem. Rev.* **2008**, *108*, 2145–2179; b) R. Tyburski, T. Liu, S. D. Glover, L. Hammarström, *J. Am. Chem. Soc.* **2021**, *143*, 560–576.
[28] R. H. Wopschall, I. Shain, *Anal. Chem.* **1967**, *39*, 1514–1527.
[29] F. Wang, S. S. Stahl, *Acc. Chem. Res.* **2020**, *53*, 561–574.
[30] J. M. Mayer, *Annu. Rev. Phys. Chem.* **2004**, *55*, 363–390.
[31] K. Ando, Y. Shimazu, N. Seki, H. Yamataka, *J. Org. Chem.* **2011**, *76* (10), 3937–3945.
[32] A. Shrestha, K. H. Hendriks, M. S. Sigman, S. D. Minteer, M. S. Sanford, *Chem. Eur. J.* **2020**, *26*, 5369–5373.
[33] S. Samaroo, C. Hengesbach, C. Bruggeman, N. G. G. Carducci, L. Mtemeri, R. J. Staples, T. Guarr, D. P. Hickey, *Nat. Chem.* **2023**, *15*, 1365–1373.
[34] CrysAlisPro 1.171.42.80a, **2023**, Rigaku Oxford Diffraction.
[35] G. M. Sheldrick, **2016**, SADABS, Version 2016/2. Bruker AXS Inc., Germany.
[36] G. M. Sheldrick, *Acta Crystallogr.* **2015**, *A71*, 3–8.
[37] O. V. Dolomanov, L. J. Bourhis, R. J. Gildea, J. A. K. Howard, H. Puschmann, *J. Appl. Crystallogr.* **2009**, *42*, 339–341.
[38] G. M. Sheldrick, *Acta Crystallogr.* **2015**, *C71*, 3–8.
[39] Mercury 2022.3.0 (Build 364735).
[40] A. J. Bard, L. R. Faulkner, *Electrochemical Methods: Fundamentals and Applications*, John Wiley & Sons Inc., 2nd Edition., **2001**.
[41] Schrödinger Release 2017–1: Epic, Schrödinger, LLC, New York, NY, **2017**.
[42] P. Pracht, F. Bohle, S. Grimme, *Phys. Chem. Chem. Phys.* **2020**, *22*, 7169–7192.
[43] User Guide to Semiempirical Tight Binding, https://xtb-docs.readthedocs.io/en/latest/contents.html.
[44] a) S. Grimme, C. Bannwarth, P. Shushkov, *J. Chem. Theory Comput.* **2017**, *13*, 1989–2009; b) C. Bannwarth, S. Ehlert, S. Grimme, *J. Chem. Theory Comput.* **2019**, *15*, 1652–1671.
[45] Y. Zhao, D. G. Truhlar, *Theor. Chem. Acc.* **2008**, *120*, 215–241.
[46] M. J. Frisch, G. W. Trucks, H. B. Schlegel, G. E. Scuseria, M. A. Robb, J. R. Cheeseman, G. Scalmani, V. Barone, G. A. Petersson, H. Nakatsuji, et al., Gaussian 16 Revision C.01. **2016**; Gaussian Inc. Wallingford CT.
[47] A. V. Marenich, C. J. Cramer, D. G. Truhlar, *J. Phys. Chem. B* **2009**, *113*, 6378–6396.
[48] P. C. Hariharan, J. A. Pople, *Theor. Chim. Acta* **1973**, *28*, 213–222.
[49] F. Weigend, F. Furche, R. Ahlrichs, *J. Chem. Phys.* **2003**, *119*, 12753–12762.
[50] A. Hashemi, R. Khakpour, A. Mahdian, M. Busch, P. Peljo, K. Laasonen, *Digital Discovery* **2023**, *2*, 1565–1576.
[51] J. Rossmeisl, A. Logadottir, J. Nørskov, *Chem. Phys.* **2005**, *319*, 178–184.
[52] M. Busch, E. Ahlberg, K. Laasonen, *ACS Omega* **2022**, *7*, 17369–17383.

Manuscript received: February 28, 2024
Accepted manuscript online: April 19, 2024
Version of record online: May 29, 2024